Journal of Applied Electrochemistry **31**: 883–889, 2001.

Diagnosis of specific surface area in fuel cell air electrodes

Z.D. WEI[1], J. TAN[1], F. YIN[1], C.G. CHENG[1], W. ZHU[1], Z.Y. TANG[2] and H.T. GUO[2]
[1]*Department of Applied Chemistry, Chongqing University, Chongqing, 400044, People's Republic of China*
[2]*Department of Applied Chemistry, Tianjin University, Tianjin, 300072, People's Republic of China*

Received 5 May 2000; accepted in revised form 4 January 2001

Key words: air electrode, mathematical model, PAFC

Abstract

A model of the air electrode used in fuel cells was developed which accounts for the diffusion of oxygen in the gas-filled pores as well as diffusion into the liquid-filled pores, and electrochemical reaction. The model was applied to the air electrode in the phosphoric acid fuel cell (PAFC) to simulate the cathode performance under a variety of conditions. Two parameters AB and AI were introduced into the model. They reflect, respectively, the effects of the interfacial surface area between the gas and liquid phases and those of the interfacial surface area between the liquid and solid phases, on the air electrode performance. AB and AI can be determined with the aid of the operating conditions and potential–current density curves of the air electrode. The main interface parameters of the air electrode can be predicted following the determination of AB and AI. The reaction rate throughout the catalyst layer was calculated by means of the model.

List of symbols

a^{g}	interfacial surface area between gas and liquid phase ($cm^2\ cm^{-3}$)
a^{l}	interfacial surface area between liquid and solid phase ($cm^2\ cm^{-3}$)
AB	parameter defined by Equation 17 ($mol\ cm^{-3}\ s^{-1}$)
AI	parameter defined by Equation 18 ($A\ cm^{-3}$)
C_l^0	solubility of oxygen in the electrolyte at 1.103×10^5 Pa ($mol\ cm^{-3}\ Pa^{-1}$)
C_c	concentration of oxygen at the catalyst surface ($mol\ cm^{-3}$)
D^{l}	diffusion coefficient of oxygen dissolved in the electrolyte ($m^2\ s^{-1}$)
D_{ij}	effective gas diffusion coefficient for component i and j at the given pressure ($m^2\ s^{-1}$)
D_{ij}^{r}	effective gas diffusion coefficient for component i and j at the reference state ($m^2\ s^{-1}$)
E	electrode potential (V)
E_r	open circuit potential for oxygen electrode (V)
e	electron
F	Faradaic constant (96,487 C mol^{-1})
G	function defined by Equation 20
H_1	Henry's law constant for oxygen ($mol\ cm^{-3}\ Pa^{-1}$)
I	current density ($A\ cm^{-2}$)
I_k	current density from experiments ($A\ cm^{-2}$)
$I_{k,model}$	current density calculated from the model ($A\ cm^{-2}$)
i	local current density ($A\ cm^{-2}$)
i^0	exchange current density ($A\ cm^{-2}$)
L_d	cathode diffusion-layer thickness (cm)
L_c	cathode reaction-layer thickness (cm)
N_1	flux of oxygen ($mol\ cm^{-2}\ s^{-1}$)
P	total pressure in the gas stream and porous backing (Pa)
P_i	partial pressure of component i (Pa)
R	gas constant (8.314 J $mol^{-1}\ K^{-1}$)
R_1^{e}	electrochemical reaction rate ($mol\ cm^{-3}\ s^{-1}$)
R_1^{p}	transport rate at interface of gas and liquid phase ($mol\ cm^{-3}\ s^{-1}$)
r	radius of pores (cm)
T	temperature (K)
T^{r}	reference temperature (K)
T_s	Tafel slope (V $decade^{-1}$)
Z	spatial coordinate (cm)

Greek symbols

δ	thickness of electrolyte film (cm)
ε	porosity
τ	tortuosity
λ	parameter in Equation 22 ($mol\ cm^{-3}\ s^{-1}$)
ω	parameter in Equation 22 ($mol\ mA^{-1}\ cm^{-1}\ s^{-1}$)
γ	linear relevant coefficient between AB and I in Equation 22

Superscripts

g	gas phase
l	liquid phase
r	reference

Subscripts

c catalyst layer

d gas diffusion layer

i species *i*, $i = 1, 2, 3$ corresponding to O_2, H_2O (g) and N_2, respectively

1. Introduction

The building of the 11 MW PAFC plant at Goi (Japan) in 1991 as a prototype marked the beginning of PAFC commercialization [1] although further capital cost reduction is still required. PAFC performance requires further improvement and to improve the performance. The activation, concentration and ohmic polarizations should be minimized. To investigate the three types of polarization, numerous and costly experiments need to be conducted. Furthermore, the interaction among the three types of polarization cannot be avoided in isolating the contribution of a particular type of polarization. Mathematical modelling of fuel cells can supply a convenient means of assessing the influence of changes in parameters and operating conditions on polarization.

The 'uniform electrolyte film', a widely accepted physical model, was first proposed by Cutlip and coworkers [2, 3]. They successively developed a so-called 'simplified model' and a 'detailed model' of the air electrode used in PAFC [4], and utilized the proposed model to simulate PAFC cathode performance. Unfortunately, the parameters of the air electrode structure and operating conditions on which Cutlip's model was established deviate from today's state-of-the-art technology. First, the pore size in the Teflon-bonded catalyst layer is much larger than that assumed in Cutlip's model [5–7]. Secondly, the equation used to calculate the current density of air electrodes in Cutlip's model was quoted from the literature of the late 1960s [8]. Also, Cutlip's model did not consider the operating condition where the gas pressure was greater than one atmosphere.

Recently, Vidts and White [9] attempted to give a general governing mathematical model for any porous electrode in an imaginary binary solution based on the 'volume-averaging technique'. Almost all models to date have taken the surface area between two phases, that is, gas–liquid and liquid–solid, as two constants. However, Zhou's experiments [10] showed that electrolyte films in Teflon-bonded porous electrodes become thinner with increasing overpotential. Experiments in this laboratory confirmed Zhou's conclusion. These phenomena raise a question about the conventional view of the interfacial surface area between two phases. The present model is based on a supposition that the interfacial surface areas between phases may not be taken as constants over a wide range of current density, rather they vary with the current density.

2. Mathematical model for PAFC cathode

A schematic of a PAFC air electrode is presented in Figure 1, showing the conceptualization of the three-phase system and the process occurring within the cathode. Typically, multilayer electrodes are used in practice, where each electrode contains a gas diffusion layer consisting of hydrophobic gas-filled pores, and a reaction layer consisting of hydrophobic gas-filled pores as well as liquid-filled pores. The major assumptions on which the model is based are as follows:

(i) Knudsen diffusion of multicomponent molecular diffusion is not considered either in the gas diffusion layer or in the reaction layer. The size of gas-filled

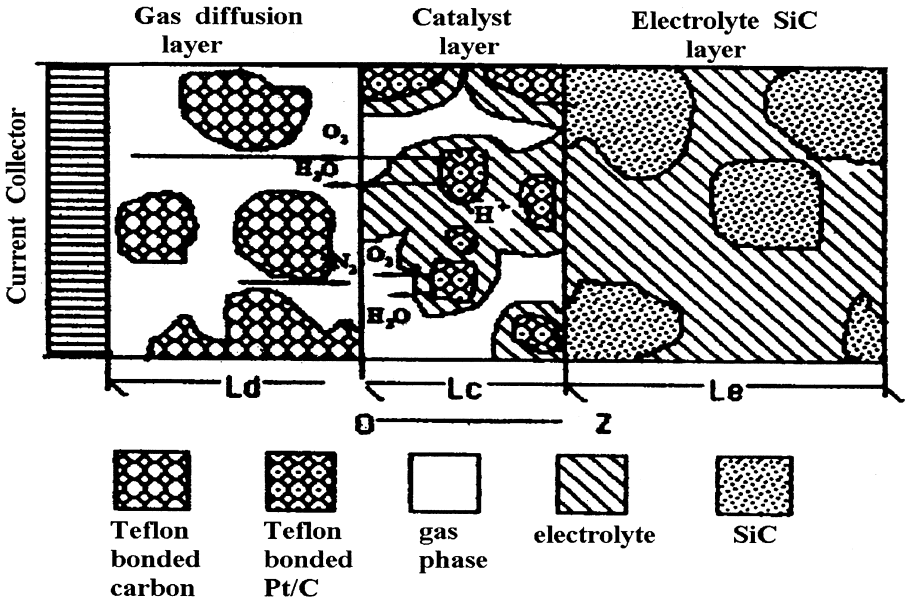

Fig. 1. Schematic of air electrode of PAFC.

pores through the whole air electrode is so large that the Knudsen diffusion can be ignored [11].

(ii) The drop in multicomponent pressure within the gas diffusion layer is negligible [12, 13].

(iii) The results of Appleby and others [14–18] concerning oxygen reduction on platinum in phosphoric acid are used to describe oxygen reduction on the platinized carbon porous PAFC electrode.

(iv) The gas-diffusion layer is described as a homogeneous continuum consisting of gas-filled layer and solid electrode framework. Similarly, the reaction layer can be described as superimposing the gas-filled and liquid-filled pores within the solid electrode framework.

(v) The potential distribution within the air electrode is not included in the model because it is very time consuming to calculate the ionic conductivity of the electrolyte film enveloping the catalyst agglomerates. In addition, it is likely that the potential distribution within an electrode is largely constant throughout the reaction layer [4].

2.1. *Gas-diffusion in the macropores of the reaction layer*

The transport equation for each species in the reaction layer is similar to that reported elsewhere [4].

$$\frac{dP_1}{dZ} = \frac{RTN_1}{P}\left(-\frac{2P_1}{D_{12}} - \frac{P_2}{D_{12}} - \frac{P_3}{D_{13}}\right) \quad (1)$$

$$\frac{dP_2}{dZ} = \frac{RTN_1}{P}\left(\frac{2P_1}{D_{12}} - \frac{P_2}{D_{12}} + \frac{2P_3}{D_{23}}\right) \quad (2)$$

$$\frac{dP_3}{dZ} = \frac{RTN_1}{P}\left(\frac{1}{D_{13}} - \frac{2}{D_{23}}\right) \quad (3)$$

The boundary conditions for the above equations are

$$P_i = P_i(0) \quad (i = 1, 2, 3) \quad (4)$$

where

$$\sum_{i=1}^{3} P_i(Z) = P \quad (5)$$

$$D_{ij} = D_{ij}^{r}\left(\frac{T}{T^{r}}\right)^{1.75}\left(\frac{P^{r}}{P}\right)\frac{\varepsilon_c^{g}}{\tau} \text{ [19]} \quad (6)$$

The values of D_{ij}^{r}, T^{r} and P^{r} are listed in Table 1.

Table 1. Experimental values of mutual diffusion coefficient for some binary gas at $p^{r} = 1.013 \times 10^{5}$ Pa [22]

i	j	T^{r}/K	D_{ij}^{r}/cm^2 s^{-1}
O_2	H_2O	352.3	0.352
	O_2	353.2	0.301
	N_2	293.2	0.220
N_2	H_2O	349.1	0.354

2.2. *Dissolution of oxygen at the interface of gas and liquid phases*

According to Henry's law, the concentration of dissolved oxygen at the interface of the gas and liquid phases is directly proportional to its partial pressure, that is,

$$C_1^0 = H_1 P_1 \quad (7)$$

2.3. *Rate of oxygen gas into the electrolyte across the interface of gas and liquid phases, R_1^p*

If the electrolyte film enveloping the agglomerates is thin in comparison with the radius of the agglomerates, Fick's law describes the diffusion of dissolved oxygen in the film

$$R_1^{p} = \frac{a^{g} D^{1}}{\delta}(H_1 P_1 - C_c) \quad (8)$$

2.4. *Electrochemical reaction rate per unit electrode volume, R_1^e*

This is expressed as

$$R_1^{e} = \frac{a^{1} i}{4F} \quad (9)$$

For the reaction,

$$O_2 + 4H^{+} + 4e^{-} = 2H_2O \quad (10)$$

Ghoneim et al. [16] investigated oxygen electroreduction on platinum in 85% D_3PO_4 and 85% H_3PO_4. They observed the same electrode behaviour in both 85% D_3PO_4 and 85% H_3PO_4. This means that H^{+} is not a reactant in the rate-determining step of Reaction 10. The reaction order of oxygen in Reaction 10 was shown to be unity [3, 17]. The work of Appleby [14, 15] and Clouser [18] showed that the Tafel slope for oxygen reduction on platinum was almost constant in concentrated H_3PO_4 from 25 °C to 250 °C. They also showed that this constant was 0.11 V per decade, that is,

$$\frac{2.3RT}{\alpha nF} = 0.11 \quad (11)$$

The backward step of Reaction 10 is negligible under normal operating conditions. Using the Butler–Volmer rate expression, we obtain the following expression for the local current density, i,

$$i = i^{0}(C_c/C_1^{0})\exp(20.91(E_r - E)) \quad (12)$$

where E_r is the reversible electrode potential of the oxygen electrode. All potentials herein are refered to the standard hydrogen electrode.

2.5. *Oxygen flux across any point in reaction layer, N_1*

As oxygen diffuses through the electrode reaction layer, some of the oxygen reacts along the way. The flux of oxygen diffusion past any point in the electrode diminishes in proportion to the rate of electrochemical reaction per unit volume of electrode, R_1^e, at that point,

$$\frac{dN_1}{dZ} = -R_1^e \tag{13}$$

At steady state, the following relationship is also found:

$$R_1^e = R_1^p \tag{14}$$

Noting that H_1 and C_1^0 are the same, Equations 8 to 14 can be combined to give the final differential equation.

$$\frac{dN_1}{dZ} = -P_1 \Big/ \left[\frac{4F}{a^1 i^0 \exp(20.91(E_r - E))} + \frac{\delta}{a^g D^1 C_1^0}\right] \tag{15}$$

The corresponding boundary condition for Equation 15 is given by

$$N_1(0) = 0 \tag{16}$$

In summary, the six governing equations for oxygen reduction in the reaction layer are Equations 1–4, 15 and 16.

3. Solution of the model

The critical structural parameters which determine the performance of porous electrodes are the interfacial surface area between the gas and the liquid phase, that is, a^g, and the area between the liquid and the solid phase, that is, a^l. These have previously been considered as constants. For example, Kimble and White [7] took a^l times the exchange current (i^0) as 0.60 A cm^{-3}, and a^g divided by the thickness of electrolyte film (δ) as 5×10^8 cm^{-2}. The above-mentioned parameters cannot be independently determined from theory or experiment. Curve fitting or more advanced optimization methods are common approaches to obtaining unknown parameters. To minimize the number of parameters to be fitted, and to avoid using questionable values of some of these, several uncertain parameters are merged into the following two new parameters:

$$AB = a^g D^1 C_1^0/\delta \tag{17}$$

$$AI = a^1 i^0 \tag{18}$$

Then Equation 15 has a new form:

$$\frac{dN_1}{dZ} = -P_1 \Big/ \left[\frac{4F}{AI \exp(20.91(E_r - E))} + \frac{1}{AB}\right] \tag{19}$$

Finally, the six governing equations for the reaction layer of a PAFC cathode are Equations 1–4, 16 and 19.

Since D^1, $C_1{}^0$ and i^0 are all constant, the changes of AB and AI actually reflect the changes of a^g/δ and a^l of an air electrode in operation, respectively. A computer program TMSTB from the Computer Center of Academia Sinica (China) was used to solve the group of differential equations. The Simplex method [20] was used to search for the optimum values of parameters AB and AI. This optimum method can automatically expand or contract search steps, which greatly accelerates the search rate of Simplex. The objective function G is defined as

$$G = \sum_{k=1}^{m} (1 - I_k/I_{k,model})^2 \tag{20}$$

where m is the number of points selected on each curve in Figure 2 [21]. I_k and $I_{k,model}$ are from the curve in Figure 2 and from the model calculation respectively. The current density $I_{k,model}$ is calculated from N_1 at the boundary of the gas diffusion layer and the reaction layer, that is,

$$I_{k,model} = N_1(0)/4F \tag{21}$$

The magnitude of G also reflects the deviation of the model from the experiments, and the smaller its value, the closer is the model to experiments. The experimental data with the operating conditions as shown in Figure 2 were used to determine the parameters AB and AI.

4. Results and discussion

The operating conditions and the relationship between the cathode potential E and the current density I, as shown in Figure 2, were substituted into the mathematical model to obtain the solution. When AB and AI are taken as constants over all current densities, an apparent deviation occurs between the current density from the model and that from the experiment, although the model does largely follow experiment, as shown in Table 2. Since Table 2 shows that the deviation becomes smaller at lower current densities, the scale of current densities was divided into two regions, from zero to 100 mA cm^{-2}, and from 100 to 300 mA cm^{-2}. The parameters AB and AI were respectively optimized in the two regions. The results are summarized in Table 3 and Table 4, which show that the difference between the model and the experiment has been markedly reduced. Using this, parameter AB and AI were further optimized point by point along each curve in Figure 2. It is surprising to find that the parameter AB is almost linear with current density at each operating gas pressure, while parameter AI is almost independent of current density. In fact, parameter AI only oscillates in the range $(4.2 \pm 5\%) \times 10^{-2}$ A cm^{-3} for all the curves in Figure 2.

As parameters AB and AI are only required to satisfy the minimum of G for a single point, that is, $m = 1$.

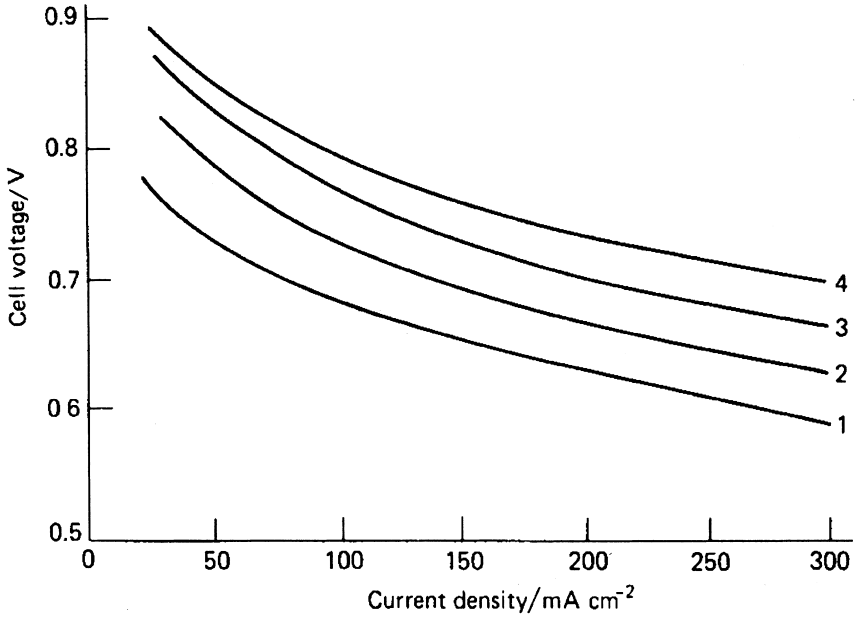

Fig. 2. Phosphoric acid fuel cell performance for a range of pressure (at start of test). Legend: (1) Atmospheric pressure, 190 °C, 0.5 mg cm^{-2} Pt on carbon; (2) 3×10^5 Pa, 190 °C, 0.5 mg cm^{-2} Pt on carbon; (3) 6×10^5 Pa, 210 °C, 0.5 mg cm^{-2} Pt on carbon; and (4) 8×10^5 Pa, 190 °C, 0.5 mg cm^{-2} Pt on carbon.

Table 2. Comparison of current densities between the experiment of Figure 2 and the model in the case of AB and AI as constants for each curve

I_k/mA cm^{-2}	$I_{k,model}$/mA cm^{-2}			
	Curve 1	Curve 2	Curve 3	Curve 4
27	24	25	25	23
35	30	28	29	30
38	33	32	33	34
50	49	48	48	48
55	57	61	60	59
74	80	88	84	80
112	136	140	149	137
188	201	214	217	215
300	269	258	253	261
$AB \times 10^4$ (mol cm^{-3} s^{-1})	1.25	1.36	1.69	1.74
$AI \times 10^2$ (A cm^{-3})	3.66	1.08	0.52	0.43
$G \times 10^2$	7.16	16.56	15.21	9.74

Table 3. Comparison between the experiment and the model as AB and AI are optimized before and after current density of 100 mA cm^{-2}, respectively

I_k/mA cm^{-2}	$I_{k,model}$/mA cm^{-2}	
	Curve 3	Curve 4
38.46	37.73	38.92
55.36	57.10	53.76
74.05	73.33	75.73
85.18	90.79	86.63
100.00	97.91	98.12
100.00	95.12	95.78
111.54	112.60	111.53
169.53	181.93	182.58
226.92	238.25	236.53
300.00	282.69	284.07

Equation 20 can be easily satisfied by a very low value of G. In general, this parameter is less than 1×10^{-14}, which means that the experimental current density is almost equal to that from the model.

Parameter AB and current density I have the following relationship:

$$AB = \lambda + \omega I \tag{22}$$

The values of λ and ω are listed in Table 5. Obviously, the physical meaning of λ is the value of AB at zero current density, while ω reflects the influence of current density on AB.

From the definition of parameter AB (i.e., $AB = a^g DC_1^0/\delta$) the variation of AB with the current density shows the relationship between a^g/δ and current density. The increase in parameter AB with current density means that the interfacial surface area between the gas and liquid phases (a^g) increases and/or the thickness of the electrolyte film (δ) decreases. Since AI is constant over the range of current density, the interfacial surface area between the liquid and the solid phase (a^l) can also be considered constant. The main part of the increases in AB is due to a decreases in electrolyte film thickness (δ) rather than an increases of the interfacial surface area between the gas and liquid phases (a^g). This novel conclusion had already been reported by Zhou and Poorten [10]. Based on the changes in electrolyte film thickness (δ), the following conclusions can be drawn: (i) The diffusion polarization of dissolved oxygen at low current density must be higher than that at high current density. (ii) The ohmic resistance of electrolyte at high current density becomes more significant than that at

Table 4. AB, AI and G in the two ranges of current densities

	0–100 mA cm^{-2}				100–300 mA cm^{-2}			
	Curve 1	Curve 2	Curve 3	Curve 4	Curve 1	Curve 2	Curve 3	Curve 4
$AI \times 10^2$/A cm^{-3}	1.483	1.897	2.40	2.40	0.873	0.784	0.864	1.116
$AB \times 10^5$/mol cm^{-3} s^{-1}	20.390	4.890	2.34	2.09	46.175	13.994	6.926	5.634
$G \times 10^2$	0.138	1.123	0.811	0.216	0.811	0.942	1.337	1.186

Table 5. Results as fitted point by point

Curve (P, T)	λ/mol cm^{-3} s^{-1}	ω/(mol mA^{-1} cm^{-1} s^{-1})*	$AI/ \times 10^2$ A cm^{-3}	γ
Curve 1 (1×10^5 Pa, 190 °C)	1.7115×10^{-5}	1.1035×10^{-6}	4.18 ± 5%	0.99942
Curve 2 (3×10^5 Pa, 190 °C)	5.7549×10^{-6}	3.6096×10^{-7}	4.23 ± 5%	0.99984
Curve 3 (6×10^5 Pa, 210 °C)	4.1548×10^{-6}	1.7613×10^{-7}	4.21 ± 5%	0.99914
Curve 4 (8×10^5 Pa, 210 °C)	3.9502×10^{-6}	1.3378×10^{-7}	4.15 ± 5%	0.99914

* The unit of I in Equation 22 is mA cm^{-2}.
G is less than 1×10^{-14} at any point for all curves.

low current density. (iii) There must be an optimum operating current density for a high power output of an air cathode on account of the diffusion of dissolved oxygen and ohmic polarization.

The influence of the operating pressure on AB, and in turn on a^g/δ, can also be observed from Table 5. The dependence of AB on current density decreases with gas operating pressure.

The flux distribution of oxygen across the catalyst layer can be converted into an index indicating the electrochemical reaction rate across the dimensionless reaction layer. The reduction of N_1 in magnitude from Z_i to $Z_i + \Delta Z$, that is, ΔN_1 (Z_i) equals the electrochemical reaction rate over the thickness ΔZ. The ratio of ΔN_1 (Z_i) to the maximum $\{\Delta N_1$ (Z_i)$\}$ as a function of the dimensionless reaction layer (Z/L_c) is shown in Figure 3, which indicates that the reaction rate is not uniform throughout the reaction layer. Although Figure 3 only displays the result at given conditions, the results at other operating conditions (T, P) and the current densities also display similar behaviour, as shown in Figure 3. The highest rate appears at the gas diffusion/catalyst layer interface. This conclusion agrees with assumption (iv), which considers the catalyst layer as a homogeneous continuum consisting of the superimposed gas-filled and liquid-filled pores within the solid electrode framework. A main difference at $Z/L_c = 0$ and at $Z/L_c = 1$ lies in the difference in oxygen concentration, which may result in a difference in oxygen electroreduction rate. This suggests that the higher operating pressure can help in making full use of precious metal catalysts in the reaction layer.

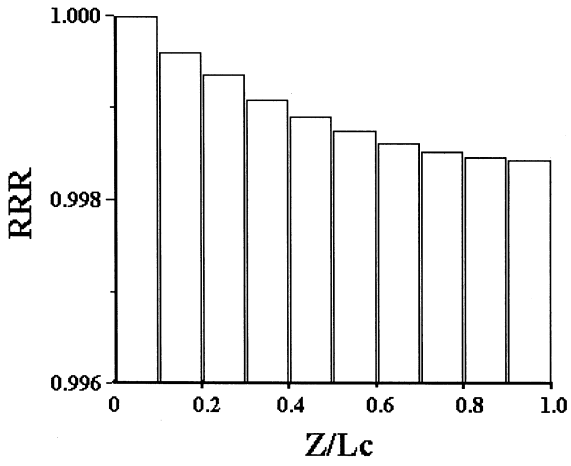

Fig. 3. Relative reaction rate (RRR) across the dimensionless reaction layer at the gas pressure of 3×10^5 Pa and at the current density of 100 mA cm^{-2}.

When AB and AI are taken as constants from zero to 300 mA cm^{-2} current density, the relative error in the current density predicted by the model is up to 16.56% relative to that given by experiment. When parameters AB and AI are fitted below and above 100 mA cm^{-2}, respectively, this error drops to less than 5%. Furthermore, if AB and AI are fitted at each single current density, the error is almost negligible. These results confirm that the interfacial surface area between the gas and the liquid phase varies with current density, in other words, with electrode potential.

It is also found that there is a linear relationship between parameter AB and current density and that parameter AI oscillates in a very narrow range for all current densities. The increase in parameter AB with current density indicates that there is an optimum current density for a high power output of the air cathode on account of the diffusion polarization of dissolved oxygen and the ohmic resistance of the electrolyte.

5. Conclusion

Parameters AB and AI, characterizing the three-phase air electrode, can be predicted with the aid of the proposed model; the critical interface parameters can then be determined.

Acknowledgements

This work was supported by the National Natural Science Foundation of China (NSFC) under Grant 29 976 047.

References

1. A.J. Appleby *J. Power Sources* **69** (1996) 153.
2. M.B. Cutlip, *Electrochim. Acta* **20** (1975) 767.
3. R.P. Iczkowski and M.B. Cutlip, *J. Electrochem. Soc.* **127** (1980) 1433.
4. S.C. Yang , M.B. Cutlip and P. Stonehart, *Electrochim. Acta* **34** (1989) 703; **35** (1990) 869.
5. K. Tomantschger and K.V. Kordesch, *J. Power Sources* **25** (1989) 195.
6. H. Fukuda, H. Abe and M. Funabashi, Eur. Patent 364, 297 (1989).
7. M.C. Kimble and R.E. White, *J. Electrochem. Soc.* **138** (1991) 3370; **139** (1992) 478.
8. R. Aris, 'Elementary Chemical Reactor Analysis' (Prentice Hall, Englewood Cliff, NJ, 1969).
9. P. Vidts and R.E. White, *J. Electrochem. Soc.* **144** (1997) 1343.
10. D.B. Zhou and H.V. Poorten, *Electrochim Acta* **40** (1995) 1819.
11. D. Culsen, *in* N.P. Cheremisinolt (Ed.), 'Handbook of Heat and Mass Transfer' Vol. 2 (Gulf Publishing, Houston, TX, 1986), p. 435.
12. Z.D. Wei, H.T. Guo and Z.Y. Tang, *Acta Phys. Chim Sinica* **12** (1996) 1022.
13. Z.D. Wei, H.T. Guo and Z.Y. Tang, *Chem. J. Chinese University* **17** (1996) 1760.
14. A.J. Appleby, *in* B.E. Coway and J.O'M. Bockris (Eds), 'Comprehensive Treaties of Electrochemistry', Vol. 6. (Plenum Press, New York, 1983), p. 173.
15. A.J. Appleby and F.R. Foulkes, 'Fuel Cell Handbook' (Van Nostrand Reinhold, New York, 1989).
16. M. Ghoneim , S. Clouser and E. Yeager, National Conference, The Electrochemical Society San Fransisco (1983), Vol. 83–1, p. 801.
17. M.R. Tarasevich, E. Yeager, *in* B.E. Coway and J.O'M. Bockris (Eds), 'Comprehensive Treaties of Electrochemistry', Vol. 7 (Plenum Press, New York, 1983), p. 301.
18. S.J. Clouser, J.C. Huang and E. Yeager 'Anomalous temperature dependence of the Tafel slopes for O_2 reduction on platinum in phosphoric acid' National Meeting, The Electrochemical Society, Montreal, May (1982), Extended Abstracts , Vol. 82–1, p. 348.
19. Y.A. Chizmadzhev and Y.G. Chirkov., *in* R.E. Yeager and J.M. Bockris (Eds), 'Comprehensive Treaties of Electrochemistry', Vol. 6 (Plenum Press, New York, 1983), p. 353.
20. Z.M. Zhou and S.Y. Tan, 'Computer Application in Chemistry and Chemical Engineering' (Qongqing University Press, Qongqing, 1996), p. 188–192.
21. D. Lindon, 'Handbook of Batteries and Fuel Cells' (McGraw-Hill, New York, 1982), p. 43–10.
22. K.S. Thomas , L.P. Robert and R.W. Charles, 'Mass Transfer' (McGraw-Hill, New York, 1975), p. 18 and p. 40.